Journal of Anatomy

J. Anat. (2015) **226**, pp215–223 doi: 10.1111/joa.12282

Predicting bite force and cranial biomechanics in the largest fossil rodent using finite element analysis

Philip G. Cox,[1] Andrés Rinderknecht[2] and R. Ernesto Blanco[3]

[1]*Department of Archaeology and Hull York Medical School, University of York, York, UK*
[2]*Museo Nacional de Historia Natural, Montevideo, Uruguay*
[3]*Facultad de Ciencias, Instituto de Física, Montevideo, Uruguay*

Abstract

Josephoartigasia monesi, from the Pliocene of Uruguay, is the largest known fossil rodent, with an estimated body mass of 1000 kg. In this study, finite element analysis was used to estimate the maximum bite force that *J. monesi* could generate at the incisors and the cheek teeth. Owing to uncertainty in the model inputs, a sensitivity study was conducted in which the muscle forces and orientations were sequentially altered. This enabled conclusions to be drawn on the function of some of the masticatory muscles. It was found that *J. monesi* had a bite of 1389 N at the incisors, rising to 4165 N at the third molar. Varying muscle forces by 20% and orientations by 10° around the medio-lateral aspect led to an error in bite force of under 35% at each tooth. Predicted stresses across the skull were only minimally affected by changes to muscle forces and orientations, but revealed a reasonable safety factor in the strength of the skull. These results, combined with previous work, lead us to speculate that *J. monesi* was behaving in an elephant-like manner, using its incisors like tusks, and processing tough vegetation with large bite forces at the cheek teeth.

Key words: bite force; cranial biomechanics; finite element analysis; *Josephoartigasia monesi*; rodent.

Introduction

The mammalian order Rodentia comprises well over 2000 extant species (Wilson & Reeder, 2005), the majority of which are small in size, i.e. under 1 kg in mass (Silva & Downing, 1995). The largest living rodent is the capybara, *Hydrochoerus hydrochaeris*, which has a body mass of around 60 kg (Mones & Ojasti, 1986). However, many extinct species of rodent, particularly those belonging to the South American families Dinomyidae and Neoepiblemidae, reached a much larger size. The largest known fossil rodent is *Josephoartigasia monesi*, a dinomyid species from the Pliocene of Uruguay (Rinderknecht & Blanco, 2008). The fossil is an almost complete skull measuring 53 cm in length, and its body mass has been estimated to be approximately 1000 kg (Rinderknecht & Blanco, 2008), although there is a degree of controversy about this figure (Blanco, 2008; Millien, 2008).

When studying fossil species, especially those of large size such as *J. monesi*, researchers are frequently interested in elucidating feeding ecology and potential bite force (e.g. McHenry et al. 2007; Bates & Falkingham, 2012).The bite force that *J. monesi* could generate at the incisors was estimated by three different methods in a previous study (Blanco et al. 2012). Using estimated muscle cross-sectional areas and measured muscle lever arms, the incisor bite force was calculated to be 959 N. Extrapolating from a measured bite force of 13 N in rats (Nies & Ro, 2004) and using estimated body mass of 1000 kg, the expected bite force of *J. monesi* was calculated as 991 N. However, using the relationship between incisor section modulus and bite force derived by Freeman & Lemen (2008), a much greater bite force of 3214 N was calculated. Blanco et al. (2012) explain this discrepancy by suggesting that the incisors of *J. monesi* may have been extremely procumbent, and thus would have experienced greater stresses during feeding, or that the incisors were used for activities other than feeding, such as digging or defence, in which other muscles, such as the neck musculature, would have been recruited. This second suggestion raises the possibility that *J. monesi* was using its incisors much as an elephant uses its tusks.

The large discrepancy in bite force estimates in Blanco et al. (2012) highlights the difficulty of determining such values in extinct organisms, in which a great deal of information, notably soft tissue data, is missing. The 'dry skull' method (Thomason, 1991) models the jaw as a simple

Correspondence
Philip G. Cox, Centre for Anatomical and Human Sciences, Hull York Medical School, University of York, Heslington, York, YO10 5DD, UK.
T: 01904 321744; E: philip.cox@hyms.ac.uk

Accepted for publication *5 January 2015*
Article published online *4 February 2015*

lever and derives bite force from jaw-closing muscle cross-sectional areas and skull dimensions. This method has been frequently used in biomechanical research (Wroe et al. 2005; Christiansen & Wroe, 2007; Ellis et al. 2009; Grandal-d'Anglade, 2010), and rests on two major simplifications – the modelling of the skull as a beam, and the placement of each muscle force at the centroid of the area used to estimate cross-sectional area of the muscle (point load method). Although a significant correlation has been shown between measured bite forces and those calculated by the dry skull method, it has also been demonstrated that the point load method tends to miscalculate muscle cross-sectional areas (Davis et al. 2010).

Many recent studies have turned to finite element analysis (FEA) to predict bite forces in mammals (Wroe et al. 2007; Bourke et al. 2008; Dumont et al. 2011; Cox et al. 2012, 2013; Oldfield et al. 2012). FEA is an engineering technique that predicts stress, strain and deformation in an object subjected to a load (Rayfield, 2007). A virtual reconstruction of an object, such as a vertebrate skull, is created that is then converted to a mesh of many smaller and simpler elements, typically cubes or tetrahedra. The object is then constrained at a number of nodes, forces are applied, and an algorithm is used to calculate the stress and strain in each element. The advantage of FEA when calculating bite forces is that, rather than modelling the skull as a beam, its entire geometry is represented. In addition, the whole attachment area of each muscle can be loaded, instead of just a single point.

The aim of this study is to shed light on the palaeoecology of the largest fossil rodent, *J. monesi*. In particular, the feeding ecology of this unusual rodent species will be investigated using FEA to predict stress distributions across the skull during biting as well as the bite force that could be generated at each tooth. Based on previous work (Blanco et al. 2012), it is hypothesised that incisor bite force predicted by FEA will be well below that predicted by the incisor section modulus. Moreover, if *J. monesi* did indeed use its incisors in a tusk-like manner, it is predicted that peak von Mises stresses in the cranium will be considerably below the yield strength of bone. As many of the FEA input parameters, particularly muscle forces and directions of pull, will have to be estimated, a sensitivity analysis will be conducted to determine which parameters have the greatest influence on bite force predictions. Not only will this enable us to assess the accuracy of the bite force predictions, but, by varying muscle forces and orientations one by one, it will also allow us to make inferences of the specific function of the each masticatory muscle in this species. Overall, these results will help us to understand the ecology of a highly unusual fossil rodent, and will demonstrate how cranial morphology and masticatory muscle configuration can impact feeding performance.

Materials and methods

Model construction

The holotype cranium of *J. monesi*, housed in the Museo Nacional de Historia Natural, Montevideo (MNHN 921), was scanned using the Somaton Sensation CT scanner at the Hospital de Clínicas 'Dr. Manuel Quintela', Montevideo. Voxels were 0.58 × 0.58 mm and slice thickness was 0.6 mm. A 3D digital reconstruction of the skull was created from the CT scans using the segmentation function of AVIZO 8.0 (Visualization Sciences Group, Burlington, MA, USA). Internal anatomy of the bone was reconstructed as being solid, that is, trabecular bone was not separated from cortical bone, as the preservation of the specimen did not allow these to be distinguished. Recent work on macaque skulls (Fitton et al. 2015) indicates that solid models perform almost identically to models with trabecular bone, although small differences in strain will occur locally in areas where trabeculae are present. Damaged parts of cranial morphology, in particular the left zygomatic arch, were reconstructed by copying and reflecting the relevant structure from the opposite side of the skull. Missing molar teeth (right P4 and M1, and left M2) were reconstructed in the same way. The missing right incisor root was reconstructed by filling in the empty alveolus. The erupted portions of both incisors were reconstructed by eye with reference to the plastic reconstruction made for a previous study of this specimen (Blanco et al. 2012). Figure 1 shows the completed reconstruction of the *J. monesi* skull. Given the level of subjectivity in the reconstruction of the incisors beyond the alveolar margin, a second reconstruction was created with 50 mm added to the tips of both incisors (maintaining the same curvature), to assess the impact of incisor morphology on bite force and feeding biomechanics. The skull and teeth were segmented separately so that different mate-

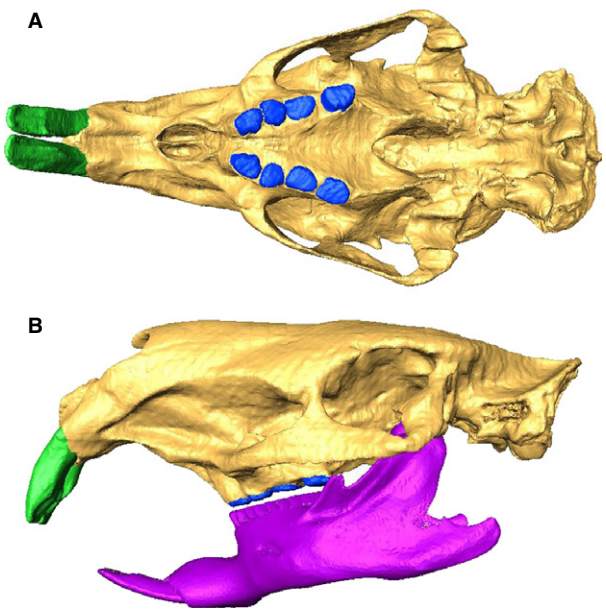

Fig. 1 Digital reconstruction of the skull of *Josephoartigasia monesi* in (A) ventral and (B) left lateral views, showing restored left zygomatic arch, incisors and molars. Scaled reconstruction of the mandible of *Lagostomus maximus* used to estimate masticatory muscle orientations also shown in lateral view.

rial properties could be applied to them. However, the component materials of the teeth (enamel, dentine and cement) could not be distinguished and so were not separately reconstructed. The reconstruction was downsampled to reduce processing time, generating an isometric voxel dimension of 1.16 mm. The downsampled reconstruction of *J. monesi* was then converted to a mesh of eight-noded cubic elements by direct voxel conversion using VOX-FE, in-house custom-built FEA software (Liu et al. 2012; available on request), resulting in a model of 1 526 906 elements. The model with elongated incisors had 1 549 885 elements. The surface reconstructions, with and without elongated incisors, and the finite element model are all available for free at http://figshare.com/authors/Philip_Cox/617885.

As no mandible exists for *J. monesi*, a scaled reconstruction of the mandible of an extant hystricognath rodent was created. The plains viscacha, *Lagostomus maximus*, was chosen as the representative hystricognath, as it was the nearest living relative of *J. monesi* for which image data was available (no mandible of *Dinomys branickii*, the sole extant dinomyid, was obtainable). The mandible of *L. maximus* is more elongate than that of *D. branickii*, and has a lower condyle; however, in these respects, it more closely resembles the mandible of *J. monesi* reconstructed in Blanco et al. (2012). The mandible of a specimen of *L. maximus* from the University Museum of Zoology, Cambridge (UMZC specimen E.3555) was imaged using the X-Tek microCT scanner at the Department of Engineering, University of Hull. Voxels were isometric and voxel dimensions were 0.069 mm. A 3D reconstruction of the mandible was created using the automatic thresholding function of AVIZO 8.0, and the resulting surface file was then scaled, rotated and translated to fit the cranial reconstruction of *J. monesi*. It can be seen from Fig. 1 that the posterior half of the *L. maximus* mandible is a good fit for *J. monesi* – the relative positions of the cheek teeth and the condyle are very similar. However, it is clear that much greater flexion would be needed in the anterior part of the mandible for incisor occlusion to occur. As all the muscle attachments are on the posterior part of the mandible, it was felt that, with appropriate sensitivity analyses (see below), the mandible of *L. maximus* could be used to estimate the masticatory muscle insertions of *J. monesi*. It should be noted that the mandibular reconstruction was not itself subjected to FEA.

Model inputs

The material properties assigned to the bone and teeth of the *J. monesi* model were based on previously published FE models of rodents (Cox et al. 2011, 2012, 2013). Bone was assigned a Young's modulus of 17 GPa and the teeth were given a Young's modulus of 30 GPa. Both materials were modelled as being linearly elastic and isotropic with a Poisson's ratio of 0.3 (Williams & Edmundson, 1984). The model was constrained in three areas: at the left and right jaw joints on the ventral surface of the zygomatic process of the squamosal; and at the biting tooth. The jaw joints were constrained in all three dimensions, but the bite point was only constrained in the direction of the bite, which was assumed to be perpendicular to the occlusal plane. The number of nodes constrained at each location varied between 140 and 521.

Loads were added to both sides of the model to represent the major muscles of mastication: superficial masseter; deep masseter; zygomaticomandibularis (ZM); infraorbital part of the zygomaticomandibularis (IOZM); temporalis; medial pterygoid; and lateral pterygoid. The layers of the masseter are here named superficial/deep/ZM following Turnbull (1970), Weijs (1973) and Cox & Jeffery (2011), as opposed to the superficial/lateral/medial nomenclature of other researchers (e.g. Wood, 1965; Woods, 1972). To facilitate comparisons with previous work, the cross-sectional areas (CSA) of the muscles were based on the estimates given in Blanco et al. (2012). In that study, bony proxies are used to determine the CSA of the '*masseter superficialis and masseter lateralis*' as a single unit, the '*masseter medialis*', and the '*temporalis*'. As the bony proxy used for the '*masseter medialis*' is the cross-section of the infraorbital foramen, it is clear that it is only the portion of this muscle attaching to the rostrum (i.e. the IOZM) that is being referred to here. In addition, the estimation of the CSA of the superficial and deep masseters, following the method of Thomason (1991), must also have included the parts of the ZM originating from the medial surface of the zygomatic arch (the anterior and posterior ZM). Thus the three muscle CSAs calculated in Blanco et al. (2012) refer to: the superficial masseter, deep masseter and ZM as a unit; the IOZM; and the temporalis. For the FE model in this study, the first of those CSAs was divided into its component muscles based on the muscle proportions measured in the capybara, *Hydrochoerus hydrochaeris* (Müller, 1933). Approximate relative CSA values for the capybara muscles were obtained by squaring the cube roots of the muscle masses. Although as absolute values these CSA values are of course highly inaccurate owing to the lack of data on fibre length, they will at least give an approximate indication of the relative sizes of the different muscle CSAs. Using the capybara CSA data as percentages, separate CSA values were obtained for the superficial masseter, deep masseter and ZM of *J. monesi* (Table 1). Similarly, CSA values for the medial and lateral pterygoid muscles were calculated for *J. monesi* based on their size relative to the other masticatory muscles in the capybara. Muscle forces (given in Table 1) were calculated by multiplying CSAs by an intrinsic muscle stress value of 0.3 N mm^{-2} (van Spronsen et al. 1989). For the accurate calculation of muscle force, CSA should be multiplied by the cosine of the pennation angle as well as intrinsic muscle stress. As pennation angles were unknown, it was not possible to include these in the force calculations. However, in most rodent masticatory muscles, the pennation angle is small, and thus the cosine is close to one (Druzinsky, 2010). The temporalis and medial pterygoid muscles have larger pennation angles and so their forces may have been overestimated, but the magnitudes of these two muscles were not found to have a large impact on bite force.

Muscle attachment sites were based on the descriptions given in Blanco et al. (2012) as well as descriptions of muscle origins and insertions in extant hystricomorph rodents (Müller, 1933; Turnbull,

Table 1 Muscle cross-sectional areas and loads applied to each side of the finite element model of *Josephoartigasia monesi*.

Muscle	CSA (cm^3)	Force (N)
Superficial masseter	22.83	685
Deep masseter	15.15	454
Zygomatico-mandibularis	12.02	360
IOZM	25.00	750
Temporalis	20.50	615
Medial pterygoid	15.85	476
Lateral pterygoid	6.57	197
Total	117.92	3537

1970; Woods & Howland, 1979; Woods & Hermanson, 1985; Hautier & Saksiri, 2009; Hautier, 2010; Cox & Jeffery, 2011). Both the IOZM and temporalis have clear fossae from which they originate on the rostrum and braincase, respectively. The deep masseter takes its origin along the length of the ventral margin of the zygomatic arch, and the origin of the superficial masseter is a small area located immediately anterior to deep masseter attachment. The ZM attaches to the medial surface of the zygomatic arch and the medial and lateral pterygoid muscles originate from the medial and lateral surfaces of the pterygoid flange, respectively. The directions of pull of the muscles were determined by placing landmarks at the centroids of the muscle insertion sites on the reconstructed mandible of *L. maximus*, which was aligned with the cranium with the teeth in occlusion (i.e. with the jaws closed; see Fig. 1). The landmarks were then uploaded to VOX-FE and used as the end points of the muscle vectors. The muscle attachment areas and vectors are shown on the FE model of *J. monesi* in Fig. 2.

Model solution and analysis

The loaded finite element model of *J. monesi* was solved for biting at each tooth, using VOX-FE. Owing to their close apposition, gnawing at the incisors was assumed always to be bilateral. Molar chewing, however, was modelled as unilateral biting on the right side. Bite force, von Mises stress patterns, and the maximum von Mises stress across the skull were recorded from each solved model. Given the approximate nature of the muscle loads, and in order to assess the influence of each muscle on bite force, the five largest muscle forces (IOZM, superficial masseter, temporalis, medial pterygoid and deep masseter) were increased and decreased by 20%, one at a time. Similarly, as muscle pull direction was based on the mandibular muscle attachment sites of a different species, the angle of the muscle vector relative to the direction of bite force was varied by 10° in both directions around the medio-lateral axis. The models with altered muscle force magnitudes and orientations were solved for biting at the incisors, premolar and third molar only (in order to represent bites at the most mesial and distal points on the cheek tooth row). In addition, a model was solved, for incisor gnawing only, with elongated incisors. Finally, based on the previous results, a model was created with all muscle forces increased by 20% and muscle vectors reoriented by 10° in the direction of increasing bite force, in order to maximise bite force, in addition to another model that minimised bite force, to produce a confidence interval for bite force estimates in *J. monesi*.

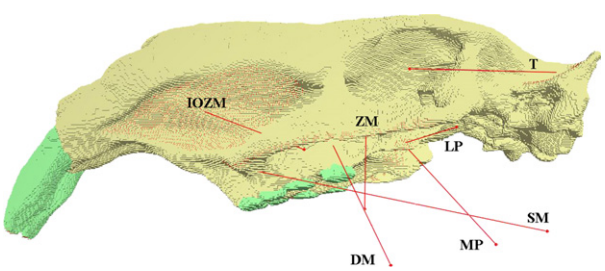

Fig. 2 Finite element model of the skull of *Josephoartigasia monesi* in left lateral view. Stippled red areas indicate muscle attachments, red arrows represent muscle vectors. DM, deep masseter; IOZM, infraorbital part of the zygomatico-mandibularis; LP, lateral pterygoid; MP, medial pterygoid; SM, superficial masseter; T, temporalis; ZM, zygomaticomandibularis.

Results

Bite force

Table 2 gives the bite force predicted by the FE model of *J. monesi* at each tooth. Bite force was calculated to be 1389 N at the incisors, rising to 2984 N at the premolar and 4165 N on the most distal tooth on the dental arcade, the third molar. The reaction forces at the working side temporo-mandibular joint are also given in Table 2. These show that, even when biting at the most distal tooth (M3), there are no distractive forces at the jaw joint that would tend to dislocate the jaw. The effect on bite force of changing the muscle force magnitudes by 20% is shown in Table 3. It can be seen that the muscles with the greatest influence on bite force are the superficial masseter, the IOZM and, to a slightly lesser degree, the deep masseter. A 20% change in the force applied by any of these three muscles will result in a 4–6% change in output bite force at either the incisors or the cheek teeth. The deep masseter appears to act equally on all teeth, whereas the superficial masseter and IOZM

Table 2 Bite force at each tooth predicted by the finite element model of *Josephoartigasia monesi*.

Biting tooth	Bite force (N)	Working side reaction force (N)	Peak von Mises stress (MPa)
I	1389	1689	24.85
PM	2984	991	23.36
M1	3298	718	27.43
M2	3625	516	31.18
M3	4165	113	39.09

I, incisor; PM, premolar; M1, first molar; M2, second molar; M3, third molar.

Table 3 Bite force at the incisor, premolar and third molar predicted by models with altered muscle load magnitudes. Percentage difference from bite force of original models (given in Table 1) calculated.

	Bite force (N)			% difference		
	I	PM	M3	I	PM	M3
SM +20%	1469	3150	4391	± 5.76	± 5.56	± 5.41
SM −20%	1309	2818	3940			
DM +20%	1447	3109	4339	± 4.16	± 4.19	± 4.17
DM −20%	1331	2859	3992			
IOZM +20%	1465	3147	4391	± 5.52	± 5.47	± 5.41
IOZM −20%	1312	2821	3940			
T + 20%	1391	2989	4171	± 0.18	± 0.15	± 0.14
T −20%	1386	2980	4160			
MP +20%	1413	3043	4256	± 1.77	± 1.97	± 2.16
MP −20%	1364	2925	4075			

I, incisor; PM, premolar; M3, third molar; SM, superficial masseter; DM, deep masseter; IOZM, infraorbital zygomaticomandibularis; T, temporalis; MP, medial pterygoid.

both have a slightly greater influence on incisor biting than on molar biting. Changes to the medial pterygoid load have much less of an effect on bite force – just a 2% difference resulting from a 20% change in muscle force. The medial pterygoid also differs from the other muscles in affecting molar bites more than incisor bites. The temporalis is unusual among the masticatory muscles in that varying its input force by 20% barely affects the output bite force at all, with just a 0.2% change being recorded.

The effect of changing muscle vector orientation on bite force shows a different pattern to that seen when changing force magnitudes (Table 4). Changing the pull direction of the IOZM has the greatest effect on bite force (7–9% difference), followed by the superficial masseter. Despite being relatively important with regard to its magnitude, the orientation of the deep masseter has minimal effect on bite force. Similarly, the orientation of the medial pterygoid appears to be largely unimportant with regard to bite force. The orientation of the temporalis was not varied in this way, as the position of the temporal fossa in relation to the jaw joint constrains its direction of pull to a narrow range of angles. The effect of superficial masseter orientation on bite force appears to be fairly consistent across all teeth, whereas the orientation of the IOZM has a greater effect on the force produced by the incisors than by the molars.

Changes to the length of the incisors had little effect on the predicted bite force. An addition of 50 mm to the tip of both incisors increased bite force from 1389 N to 1397 N – an increase of just < 1%.

Based on the above results, an estimate of the maximum error in bite force was calculated by increasing the load magnitude of the superficial masseter, deep masseter, IOZM and medial pterygoid by 20%, and reorienting the vector of the superficial masseter and IOZM by 10° towards the rostrum. A second model was constructed with the opposite loading conditions. The resulting bite forces are given in Table 5. It can be seen that, given an uncertainty of ± 20% in muscle force magnitude and ± 10° in muscle force vector, *J. monesi* would have been able to generate a bite force of between 967 and 1850 N at the incisors, between 2082 and 3970 N at the premolar, and between 2914 and 5534 N at the third molar. This represents a fairly consistent error across the teeth of ± 30–33% from the bite forces predicted by the original models.

Table 4 Bite force at the incisor, premolar and third molar predicted by models with altered muscle vector orientations. Positive angles represent rotations around the medio-lateral axis in an anterior direction. Percentage difference from bite force of original models (given in Table 1) calculated. Muscle orientations measured in the parasagittal plane.

	Bite force (N)			% difference		
	I	PM	M3	I	PM	M3
SM +10°	1467	3154	4401	5.63	5.68	5.66
SM −10°	1287	2766	3863	−7.31	−7.31	−7.26
DM +10°	1386	2980	4161	−0.21	−0.15	−0.11
DM −10°	1383	2970	4144	−0.42	−0.48	−0.52
IOZM +10°	1494	3205	4470	7.56	7.41	7.31
IOZM −10°	1264	2722	3804	−8.96	−8.79	−8.67
MP +10°	1378	2964	4140	−0.76	−0.67	−0.61
MP −10°	1397	2998	4181	0.58	0.46	0.37

I, incisor; PM, premolar; M3, third molar; SM, superficial masseter; DM, deep masseter; IOZM, infraorbital zygomaticomandibularis; MP, medial pterygoid.

Stress distribution

Figure 3 shows the distribution of von Mises stresses across the skull during biting at the different teeth. It can be seen that bites on all teeth produce high stresses on the zygomatic arch and the zygomatic process of the frontal bone. Incisor bites also generate a small region of high stress on the ventral rostrum around the incisive foramina, as well as a highly stressed area in the postero-dorsal part of the orbit. Moderate stresses are found across the rest of the orbital wall and along the dorsal part of the skull from the nares to the posterior orbital margin. Premolar bites produce lower stresses than incisor bites in the orbit and skull roof, but stress across the skull then increases as the bite point moves further along the molar tooth row towards the jaw joint. Bites on the third molar generate high stresses in the anterior orbital wall, the posterior part of the rostrum, the alisphenoid bone in the postero-ventral part of the orbit, and in a small zone on the skull roof dorsal to the posterior orbital margin. In unilateral molar bites, the von Mises stresses are generally lower on the balancing side, although still high in the zygomatic arch. Peak von Mises stresses in the cranium (excluding the teeth) are 24.8 MPa in incisor bites, 23.4 MPa in premolar bites, and between 27.4 and 39.1 MPa in molar bites (Table 2).

Despite notable effects on bite force, changing the length of the incisors or the magnitude of muscle force loaded on the model has no identifiable impact on the distribution of

Table 5 Minimum and maximum bite force at each tooth predicted by the finite element model of *Josephoartigasia monesi.*

Biting tooth	Minimum bite force (N)	Maximum bite force (N)
I	967	1850
PM	2082	3970
M1	2301	4389
M2	2533	4819
M3	2914	5534

I, incisor; PM, premolar; M1, first molar; M2, second molar; M3, third molar.

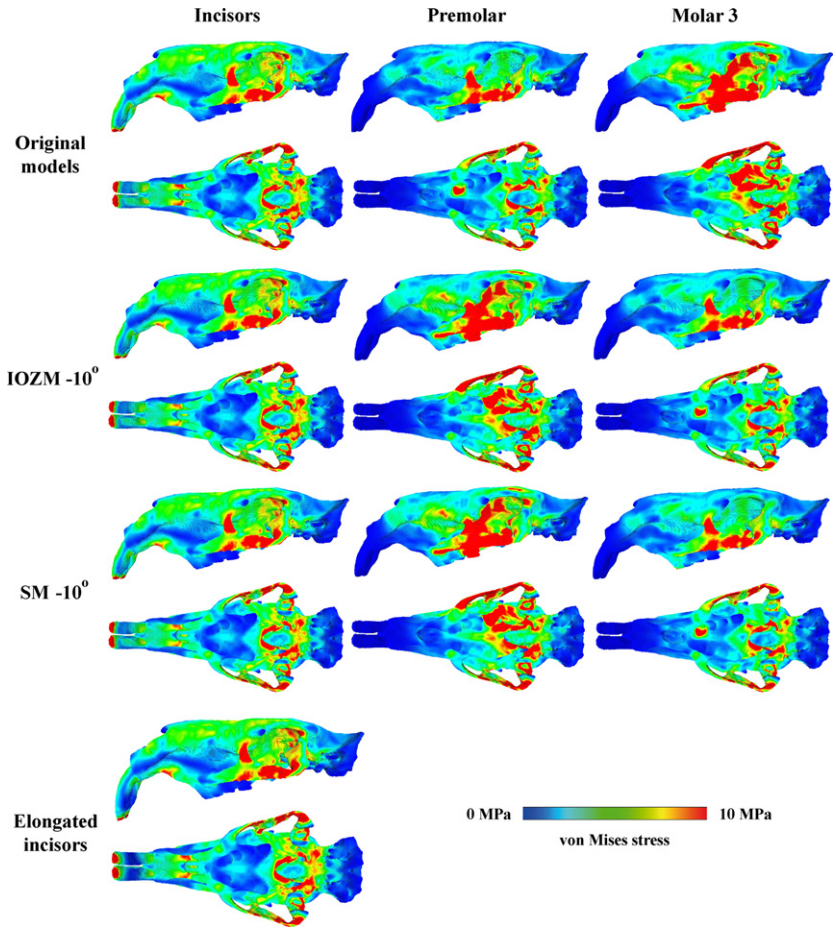

Fig. 3 Predicted distribution of von Mises stresses across the skull of *Josephoartigasia monesi* during bites at the incisors (first column), the left premolar (second column) and the left third molar (third column), shown in left lateral and ventral views. Lines 1 and 2, models with original orientation of muscle vectors; lines 3 and 4, IOZM vector rotated 10° posteriorly; lines 5 and 6, superficial masseter (SM) vector rotated 10° posteriorly; lines 7 and 8, model with incisors elongated by 50 mm.

von Mises stresses across the skull. Reorientation of the superficial masseter and IOZM vectors by 10° posteriorly slightly reduces the stresses around the incisive foramina during incisor biting, and reduces stresses on the rostrum immediately superior to the IOZM attachment area during biting at the third molar (Fig. 3). Otherwise, changing the orientation of the muscle vectors appears to have little impact on von Mises stress distributions.

Discussion

Cranial biomechanics

The solved FE models presented here indicate that, based on previously estimated muscle forces (Blanco et al. 2012), *J. monesi* would have been able to generate a bite force of approximately 1389 N at the incisors, and between 2984 and 4165 N at the cheek teeth (Table 2). Although no explicit validation can be performed on these values, previous work has shown that bite forces predicted by FE models of rodent (rat and guinea pig) crania closely match forces measured by *in vivo* experiments (Cox et al. 2012). The incisor bite force is around 40% higher than the 959 N calculated by Blanco et al. (2012). This is partly due to the higher total muscle force in this study resulting from the addition of forces representing the (non-infraorbital) ZM and medial and lateral pterygoid muscles. However, the total muscle CSA is only 24% higher in the FE models in this study than in the Blanco et al. (2012) reconstruction, so other factors are likely to be contributing to the increased bite force as well, such as the orientation of the muscle vectors.

It should be noted that the incisor bite force estimated by this study is substantially lower than the 3214 N estimated from incisor cross-sectional area by Blanco et al. (2012). Even in light of the refined bite force estimations here, it still appears that the incisors of *J. monesi* were overengineered with respect to feeding; that is, they could resist much greater forces than could ever be generated by the masticatory muscles. Thus, it has been suggested that *J. monesi* may have regularly used its incisors for activities other than feeding, such as digging for food or defence against predators, both of which would generate higher

forces at the incisors by using other muscles such as the neck musculature. The peak von Mises stresses predicted here certainly indicate that the skull could withstand activities generating greater forces than produced by feeding. The maximum stress calculated for incisor biting was 24.9 MPa, which is very much lower than both the compressive and tensile yield stresses of bone (180 and 130 MPa, respectively; Cezayirilioglu et al. 1985). Overall, the peak stresses experienced by the skull of *J. monesi* are quite high, exceeding those predicted for felids and canids (5.6–21.8 MPa; Thomason, 1991), and for the lion and *Smilodon* (< 20 MPa; McHenry et al. 2007). However, even the peak von Mises stress predicted for biting at the third molar (39.1 MPa) is exceeded by many small mammals during feeding, e.g. bats (Dumont et al. 2005) and callitrichid primates (Bourke et al. 2008). Unfortunately, data on cranial stress during feeding is lacking for large mammals, so it is not possible to ascertain whether *J. monesi* was unusual in this regard, but it is clear that there was a considerable margin of safety in the skull with respect to feeding behaviour.

The molar bite forces of *J. monesi* have not been estimated before and show an increase as the bite point moves closer to the jaw joint. Comparing the bite forces here with those predicted by previous FE studies on rodents (Cox et al. 2012, 2013), it can be seen that the ratio of premolar bite force to incisor bite force in *J. monesi* (2.15 : 1) is similar to that found in guinea pigs (2.10 : 1) but higher than most other rodents such as squirrels (1.86 : 1) and the Laotian rock rat (1.84 : 1). Beyond the premolar, the increase in bite force along the tooth row is relatively modest in *J. monesi*. The M3:PM bite force ratio is just 1.40 : 1, very similar to that seen in *Laonastes aenigmamus*, but lower than that found in *Sciurus carolinensis* and *Cavia porcellus* (1.80 : 1 and 1.72 : 1, respectively). These bite force ratios are reflective of the skull morphology of *J. monesi*: the extended rostrum and elongated diastema result in the disparity between premolar and incisor bite forces, whereas the relatively short molar tooth row leads to similar bite forces along all the cheek teeth.

It should be noted that the bite forces predicted here are based on maximal activation of all masticatory muscles on both sides of the jaw. Greaves (1978) proposed a model in which balancing side muscle forces are reduced at the distal molars to counteract distractive forces at the working side jaw joint, thus resulting in the generation of a similar bite force all along the molar tooth row. This is not the case in this model of *J. monesi*, in which the reaction force at the jaw joint on the working side is positive at all bites, including those on the third molar (Table 2). Furthermore, the reduced length of the tooth row means that the difference between bite force produced at the mesial and distal teeth is much less than it would be in the selenodont artiodactyls on which Greaves based his model. Nevertheless, it has been shown in guinea pigs that the balancing side muscle forces tend to be less than those of the working side during unilateral chewing (Byrd, 1981), so the results here should be interpreted as maximum possible bite forces rather than 'normal' chewing forces.

The lack of soft tissue data for *J. monesi* means, of course, that the bite forces predicted by the FE models are only estimates and have a degree of uncertainty surrounding them. The sensitivity analysis conducted here seeks to quantify that uncertainty. Taking all masticatory muscles into account, assuming an uncertainty of $\pm$ 20% in muscle force magnitude and $\pm$ 10° in muscle force vector, the bite forces reported in Table 2 have an error of $\pm$ 30–33%. This equates to a range of approximately 900 N for incisor bite forces, rising to 2600 N at the third molar. Although the ranges are large, they do give an indication of the magnitude of bite that *J. monesi* was able to deliver at each tooth. It is clear that the bite force of *J. monesi* was very large in absolute terms, at all teeth. Even with the assumptions that lead to the lowest bite forces (Table 5), the forces produced by *J. monesi* at the cheek teeth are still higher than all the canine bite forces estimated by Wroe et al. (2005) for some of the largest and most powerful carnivoran species. Indeed, the molar bite forces predicted for *J. monesi* are of similar magnitude to those measured at the molariform tooth of some of the largest crocodilian species (Erickson et al. 2012).

Blanco (2008) suggested that, owing to its short molar tooth row compared with its cranial length, *J. monesi* was not a good grazer and primarily only fed on soft plants. Isotopic analysis of fossil tooth enamel indicates that *J. monesi* and other large rodents fed almost exclusively on C_3 plants (Higgins et al. 2011). The very large molar bite forces predicted here indicate that *J. monesi* could feed on a wide variety of plant material, hard or soft. This prediction, combined with peak cranial stresses well below the yield stress of bone and the finding that the incisors were overengineered with respect to the bite forces generated by the masticatory muscles, indicates that *J. monesi* may have been behaving in a similar manner to an elephant. That is, it could process a broad selection of tough vegetation with the short molar tooth row, while using its unusually strong incisors like tusks for defence and digging for roots. Unfortunately, no *in vivo* bite force measurements exist for large herbivores, so direct comparisons with the bite force of elephants or other large herbivores are not possible.

Muscle function

The sensitivity analyses enable the determination of which muscles have the greatest impact on feeding biomechanics. In terms of the magnitude of muscle force, the superficial masseter has the greatest effect on bite force, followed by the IOZM and the deep masseter. This demonstrates that it is not simply the largest muscles that have the greatest influence. Indeed, the third largest muscle of mastication,

the temporalis, has an almost negligible impact on bite force, which may be due to its largely horizontal direction of pull. Thus, the primary role of the temporalis in *J. monesi* may be something other than force generation. Electromyography studies on rats (Hiiemae, 1971) and hamsters (Gorniak, 1977) have suggested that the temporalis in rodents may principally act to retract the lower jaw. Alternatively, from work on the guinea pig, it has been proposed that the rodent temporalis functions as a counterbalance to lateral translation of the mandible (Byrd, 1981). It is likely that the fibres of the temporalis in *J. monesi* actually change direction from largely horizontal to a more vertical orientation, as they run over the zygomatic process of the squamosal. Such a morphology was also noted in *Hystrix* by Turnbull (1970), who suggested that it allowed the temporalis to position the mandible with great precision. This would compensate for the lack of precision supplied by the jaw joint owing to the open glenoid fossa, which is needed for the characteristic antero-posterior movements of the jaw found in rodents. In comparison, the size of the deep masseter, which is only the fifth largest muscle of mastication in *J. monesi*, has quite a considerable effect on bite force, probably owing to its strongly vertical mode of action. This is consistent with the calculations of Turnbull (1970), who found that the masseter of rodents contributed between 15 and 36% more to bite force than would be expected based on muscle mass alone. This supports the suggestion that the deep masseter is responsible for the power stroke of mastication in rodents (Hiiemae, 1971).

In terms of the orientation of muscle pull, the muscles with the greatest influence on bite force were (in order) the IOZM, superficial masseter and the temporalis. In contrast, a change of 10° in the orientation of the medial pterygoid and deep masseter muscle had very little effect; the bite force was altered by $< 1\%$. It seems that bite force is most sensitive to changes in the vectors of those muscles which form the greatest angle with the bite force vector, such as the superficial masseter and IOZM. A change of 10° in the orientation of these muscles can cause a large change in the dorsal component of pull and thus can have a large impact on the force generated at the teeth, compared with the negligible change in bite force generated by re-orienting the deep masseter or medial pterygoid, both of which are almost parallel to the direction of bite force. However, it should be noted that the superficial masseter and IOZM are also the largest masticatory muscles and so would be expected to have a greater effect on bite force based on load magnitudes alone. This notwithstanding, the IOZM is clearly an important muscle of mastication in *J. monesi*, with changes to its direction of pull leading to differences in bite force of between 7 and 9%. A similar result was found in a study of the Laotian rock rat (Cox et al. 2013) in which the position of IOZM, and by extension its force orientation, was found to affect bite force by around 10% at all teeth. The results from this study indicate that the IOZM may affect incisor biting slightly more than molar biting in *J. monesi*.

Overall, when estimating bite force in *J. monesi*, and probably most caviomorph rodents, the accuracy of the estimate is most dependent on the accuracy of the orientation of the IOZM, and superficial masseter. In addition, the accuracy of the muscle force data for the masseter complex (superficial masseter, deep masseter and IOZM) is also important. The size of the temporalis and medial pterygoid, and the orientation of the deep masseter and medial pterygoid have little effect on the results. Surprisingly, the reconstructed length of the incisors had very little effect on the estimation of bite force, which is encouraging for researchers wishing to study feeding biomechanics of extinct taxa only known from damaged specimens. Despite the large variation in bite force with muscle input parameters, few differences were noticed in the von Mises stress distributions across the skull among the models solved as part of the sensitivity analysis (Fig. 3). It appears that the major driver of stress pattern is the geometry of the skull itself, rather than the relative magnitudes of the muscle forces or the orientation of the muscle force vectors.

Acknowledgements

The authors thank the personnel of the Radiology Department in the Hospital de Clínicas 'Dr. Manuel Quintela' for CT scanning the *J. monesi* specimen; and Professor Michael Fagan and Mrs Sue Taft (Department of Engineering, University of Hull) for microCT scanning the *L. maximus* mandible. P.G.C. is grateful to Dr Laura Fitton for assistance with model building and the VOX-FE software. The authors also thank two anonymous reviewers whose comments greatly improved the manuscript.

Author contributions

P.G.C. designed and carried out the study. A.R. and R.E.B. arranged CT scanning of the specimen. All authors analysed the results and contributed to the writing and editing of the manuscript.

References

Bates KT, Falkingham PL (2012) Estimating maximum bite performance in *Tyrannosaurus rex* using multi-body dynamics. *Biol Lett* **8**, 660–664.

Blanco RE (2008) The uncertainties of the largest fossil rodent. *Proc R Soc B* **275**, 1957–1958.

Blanco RE, Rinderknecht A, Lecuona G (2012) The bite force of the largest fossil rodent (Hystricognathi, Caviomorpha, Dinomyidae). *Lethaia* **45**, 157–163.

Bourke J, Wroe S, Moreno K, et al. (2008) Effects of gape and tooth position on bite force and skull stress in the dingo (*Canis lupus dingo*) using a 3-dimensional finite element approach. *PLoS ONE* **3**, e2200.

Byrd KE (1981) Mandibular movement and muscle activity during mastication in the guinea pig (*Cavia porcellus*). *J Morphol* **170**, 147–169.

Cezayirilioglu H, Bahniuk E, Davy DT, et al. (1985) Anisotropic yield behaviour of bone under combined axial force and torque. *J Biomech* **18**, 61–69.

Christiansen P, Wroe S (2007) Bite forces and evolutionary adaptations to feeding ecology in carnivores. *Ecology* **88**, 347–358.

Cox PG, Jeffery N (2011) Reviewing the jaw-closing musculature in squirrels, rats and guinea pigs with contrast-enhanced microCT. *Anat Rec* **294**, 915–928.

Cox PG, Fagan MJ, Rayfield EJ, et al. (2011) Finite element modelling of squirrel, guinea pig and rat skulls: using geometric morphometrics to assess sensitivity. *J Anat* **219**, 696–709.

Cox PG, Rayfield EJ, Fagan MJ, et al. (2012) Functional evolution of the feeding system in rodents. *PLoS ONE* **7**, e36299.

Cox PG, Kirkham J, Herrel A (2013) Masticatory biomechanics of the Laotian rock rat, *Laonastes aenigmamus*, and the function of the zygomaticomandibularis muscle. *PeerJ* **1**, e160.

Davis JL, Santana SE, Dumont ER, et al. (2010) Predicting bite force in mammals: two-dimensional *versus* three-dimensional lever models. *J Exp Biol* **213**, 1844–1851.

Druzinsky RE (2010) Functional anatomy of incisal biting in *Aplodontia rufa* and sciuromorph rodents – Part 2: sciuromorphy is efficacious for production of force at the incisors. *Cells Tissues Organs* **192**, 50–63.

Dumont ER, Piccirillo J, Grosse IR (2005) Finite-element analysis of biting behaviour and bone stress in the facial skeletons of bats. *Anat Rec Part A* **283A**, 319–330.

Dumont ER, Davis JL, Grosse IR, et al. (2011) Finite element analysis of performance in the skulls of marmosets and tamarins. *J Anat* **218**, 151–162.

Ellis JL, Thomason J, Kebreab E, et al. (2009) Cranial dimensions and forces of biting in the domestic dog. *J Anat* **214**, 362–373.

Erickson GM, Gignac PM, Steppan SJ, et al. (2012) Insights into the ecology and evolutionary success of crocodilians revealed through bite-force and tooth-pressure experimentation. *PLoS ONE* **7**, e31781.

Fitton LC, Prôa M, Rowland C, et al. (2015) The impact of simplifications on the performance of a finite element model of a *Macaca fascicularis* cranium. *Anat Rec* **298**, 107–121.

Freeman PW, Lemen CA (2008) A simple morphological predictor of bite force in rodents. *J Zool* **275**, 418–422.

Gorniak GC (1977) Feeding in golden hamsters, *Mesocricetus auratus*. *J Morphol* **154**, 427–458.

Grandal-d'Anglade A (2010) Bite force of the extinct Pleistocene cave bear *Ursus spelaeus* Rosenmuller from Europe. *Comp Rend Palevol* **9**, 31–37.

Greaves WS (1978) The jaw lever system in ungulates: a new model. *J Zool* **184**, 271–285.

Hautier L (2010) Masticatory muscle architecture in the gundi, *Ctenodactylus vali* (Mammalia: Rodentia). *Mammalia* **74**, 153–162.

Hautier L, Saksiri S (2009) Masticatory muscle architecture in the Laotian rock rat *Laonastes aenigmamus* (Mammalia: Rodentia): new insights into the evolution of hystricognathy. *J Anat* **215**, 401–410.

Higgins P, Croft D, Bostelmann E, et al. (2011) Paleodiet and paleoenvironment of fossil giant rodents from Uruguay. *J Vert Paleo* **31**, 125.

Hiiemae K (1971) The structure and function of the jaw muscles in the rat (*Rattus norvegicus* L.) III. The mechanics of the muscles. *Zool J Linn Soc* **50**, 111–132.

Liu J, Shi L, Fitton LC, et al. (2012) The application of muscle wrapping to voxel-based finite element models of skeletal structures. *Biomech Model Mechanobiol* **11**, 35–47.

McHenry CR, Wroe S, Clausen PD, et al. (2007) Supermodeled saberat, predatory behaviour in *Smilodon fatalis* revealed by high-resolution 3D computer simulation. *Proc Natl Acad Sci U S A* **104**, 16010–16015.

Millien V (2008) The largest among the smallest: the body mass of the giant rodent *Josephoartigasia monesi*. *Proc R Soc B* **275**, 1953–1955.

Mones A, Ojasti J (1986) *Hydrochoerus hydrochaeris*. *Mammalian Species* **264**, 1–7.

Müller A (1933) Die Kaumuskulatur des *Hydrochoerus capybara* und ihre Bedeutung für die Formgestaltung des Schädels. *Morphol Jahrb* **72**, 1–59.

Nies M, Ro JY (2004) Bite force measurement in awake rats. *Brain Res Protoc* **12**, 180–185.

Oldfield CC, McHenry CR, Clausen PD, et al. (2012) Finite element analysis or ursid cranial mechanics and the prediction of feeding behaviour in the extinct giant *Agriotherium africanum*. *J Zool* **286**, 163–170.

Rayfield EJ (2007) Finite element analysis and understanding the biomechanics and evolution of living and fossil organisms. *Ann Rev Earth Planet Sci* **35**, 541–576.

Rinderknecht A, Blanco RE (2008) The largest fossil rodent. *Proc R Soc B* **275**, 923–928.

Silva M, Downing JA (1995) *CRC Handbook of Mammalian Body Masses*. New York: CRC.

van Spronsen PH, Weijs WA, Valk J, et al. (1989) Comparison of jaw-muscle bite-force cross-sections obtained by means of magnetic resonance imaging and high-resolution CT scanning. *J Dent Res* **68**, 1765–1770.

Thomason JJ (1991) Cranial strength in relation to estimated biting forces in some mammals. *Can J Zool* **69**, 2326–2333.

Turnbull WD (1970) Mammalian masticatory apparatus. *Fieldiana (Geol)* **18**, 147–356.

Weijs WA (1973) Morphology of muscles of mastication in the Albino rat, *Rattus norvegicus* (Berkenhout, 1769). *Acta Morphol Neerl-Scand* **11**, 321–340.

Williams KR, Edmundson JT (1984) Orthodontic tooth movement analysed by the finite element method. *Biomaterials* **5**, 347–351.

Wilson DE, Reeder DM (2005) *Mammal Species of the World*. Baltimore: Johns Hopkins Press.

Wood AE (1965) Grades and clades among rodents. *Evolution* **19**, 115–130.

Woods CA (1972) Comparative myology of jaw, hyoid and pectoral appendicular regions of New and Old World hystricomorph rodents. *Bull Am Mus Nat Hist* **147**, 115–198.

Woods CA, Hermanson JW (1985) Myology of hystricognath rodents: an analysis of form, function and phylogeny. In: *Evolutionary Relationships among Rodents: A Multidisciplinary Analysis* (eds Luckett WP, Hartenberger J-L), pp. 685–712. New York: Plenum Press.

Woods CA, Howland EB (1979) Adaptive radiation of capromyid rodents: anatomy of the masticatory apparatus. *J Mammal* **60**, 95–116.

Wroe S, McHenry C, Thomason J (2005) Bite club: comparative bite force in big biting mammals and the prediction of predatory behaviour in fossil taxa. *Proc R Soc B* **272**, 619–625.

Wroe S, Clausen P, McHenry C, et al. (2007) Computer simulation of feeding behaviour in the thylacine and dingo as a novel test for convergence and niche overlap. *Proc R Soc B* **274**, 2819–2828.